Study of the decay and production properties of $D_{s1}(2536)$ and $D_{s2}^*(2573)$

M. Ablikim[1], M. N. Achasov[4,c], P. Adlarson[76], O. Afedulidis[3], X. C. Ai[81], R. Aliberti[35], A. Amoroso[75A,75C], Q. An[72,58,a], Y. Bai[57], O. Bakina[36], I. Balossino[29A], Y. Ban[46,h], H.-R. Bao[64], V. Batozskaya[1,44], K. Begzsuren[32], N. Berger[35], M. Berlowski[44], M. Bertani[28A], D. Bettoni[29A], F. Bianchi[75A,75C], E. Bianco[75A,75C], A. Bortone[75A,75C], I. Boyko[36], R. A. Briere[5], A. Brueggemann[69], H. Cai[77], X. Cai[1,58], A. Calcaterra[28A], G. F. Cao[1,64], N. Cao[1,64], S. A. Cetin[62A], X. Y. Chai[46,h], J. F. Chang[1,58], G. R. Che[43], Y. Z. Che[1,58,64], G. Chelkov[36,b], C. Chen[43], C. H. Chen[9], Chao Chen[55], G. Chen[1], H. S. Chen[1,64], H. Y. Chen[20], M. L. Chen[1,58,64], S. J. Chen[42], S. L. Chen[45], S. M. Chen[61], T. Chen[1,64], X. R. Chen[31,64], X. T. Chen[1,64], Y. B. Chen[1,58], Y. Q. Chen[34], Z. J. Chen[25,i], Z. Y. Chen[1,64], S. K. Choi[10], G. Cibinetto[29A], F. Cossio[75C], J. J. Cui[50], H. L. Dai[1,58], J. P. Dai[79], A. Dbeyssi[18], R. E. de Boer[3], D. Dedovich[36], C. Q. Deng[73], Z. Y. Deng[1], A. Denig[35], I. Denysenko[36], M. Destefanis[75A,75C], F. De Mori[75A,75C], B. Ding[67,1], X. X. Ding[46,h], Y. Ding[40], Y. Ding[34], J. Dong[1,58], L. Y. Dong[1,64], M. Y. Dong[1,58,64], X. Dong[77], M. C. Du[1], S. X. Du[81], Y. Y. Duan[55], Z. H. Duan[42], P. Egorov[36,b], Y. H. Fan[45], J. Fang[1,58], J. Fang[59], S. S. Fang[1,64], W. X. Fang[1], Y. Fang[1], Y. Q. Fang[1,58], R. Farinelli[29A], L. Fava[75B,75C], F. Feldbauer[3], G. Felici[28A], C. Q. Feng[72,58], J. H. Feng[59], Y. T. Feng[72,58], M. Fritsch[3], C. D. Fu[1], J. L. Fu[64], Y. W. Fu[1,64], H. Gao[64], X. B. Gao[41], Y. N. Gao[46,h], Yang Gao[72,58], S. Garbolino[75C], I. Garzia[29A,29B], L. Ge[81], P. T. Ge[19], Z. W. Ge[42], C. Geng[59], E. M. Gersabeck[68], A. Gilman[70], K. Goetzen[13], L. Gong[40], W. X. Gong[1,58], W. Gradl[35], S. Gramigna[29A,29B], M. Greco[75A,75C], M. H. Gu[1,58], Y. T. Gu[15], C. Y. Guan[1,64], A. Q. Guo[31,64], L. B. Guo[41], M. J. Guo[50], R. P. Guo[49], Y. P. Guo[12,g], A. Guskov[36,b], J. Gutierrez[27], K. L. Han[64], T. T. Han[1], F. Hanisch[3], X. Q. Hao[19], F. A. Harris[66], K. K. He[55], K. L. He[1,64], F. H. Heinsius[3], C. H. Heinz[35], Y. K. Heng[1,58,64], C. Herold[60], T. Holtmann[3], P. C. Hong[34], G. Y. Hou[1,64], X. T. Hou[1,64], Y. R. Hou[64], Z. L. Hou[1], B. Y. Hu[59], H. M. Hu[1,64], J. F. Hu[56,j], S. L. Hu[12,g], T. Hu[1,58,64], Y. Hu[1], G. S. Huang[72,58], K. X. Huang[59], L. Q. Huang[31,64], X. T. Huang[50], Y. P. Huang[1], Y. S. Huang[59], T. Hussain[74], F. Hölzken[3], N. Hüsken[35], N. in der Wiesche[69], J. Jackson[27], S. Janchiv[32], J. H. Jeong[10], Q. Ji[1], Q. P. Ji[19], W. Ji[1,64], X. B. Ji[1,64], X. L. Ji[1,58], Y. Y. Ji[50], X. Q. Jia[50], Z. K. Jia[72,58], D. Jiang[1,64], H. B. Jiang[77], P. C. Jiang[46,h], S. S. Jiang[39], T. J. Jiang[16], X. S. Jiang[1,58,64], Y. Jiang[64], J. B. Jiao[50], J. K. Jiao[34], Z. Jiao[23], S. Jin[42], Y. Jin[67], M. Q. Jing[1,64], X. M. Jing[64], T. Johansson[76], S. Kabana[33], N. Kalantar-Nayestanaki[65], X. L. Kang[9], X. S. Kang[40], M. Kavatsyuk[65], B. C. Ke[81], V. Khachatryan[27], A. Khoukaz[69], R. Kiuchi[1], O. B. Kolcu[62A], B. Kopf[3], M. Kuessner[3], X. Kui[1,64], N. Kumar[26], A. Kupsc[44,76], W. Kühn[37], J. J. Lane[68], L. Lavezzi[75A,75C], T. T. Lei[72,58], Z. H. Lei[72,58], M. Lellmann[35], T. Lenz[35], C. Li[43], C. Li[47], C. H. Li[39], Cheng Li[72,58], D. M. Li[81], F. Li[1,58], G. Li[1], H. B. Li[1,64], H. J. Li[19], H. N. Li[56,j], Hui Li[43], J. R. Li[61], J. S. Li[59], K. Li[1], K. L. Li[19], L. J. Li[1,64], L. K. Li[1], Lei Li[48], M. H. Li[43], P. R. Li[38,k,l], Q. M. Li[1,64], Q. X. Li[50], R. Li[17,31], S. X. Li[12], T. Li[50], W. D. Li[1,64], W. G. Li[1,a], X. Li[1,64], X. H. Li[72,58], X. L. Li[50], X. Y. Li[1,64], X. Z. Li[59], Y. G. Li[46,h], Z. J. Li[59], Z. Y. Li[79], C. Liang[42], H. Liang[1,64], H. Liang[72,58], Y. F. Liang[54], Y. T. Liang[31,64], G. R. Liao[14], Y. P. Liao[1,64], J. Libby[26], A. Limphirat[60], C. C. Lin[55], D. X. Lin[31,64], T. Lin[1], B. J. Liu[1], B. X. Liu[77], C. Liu[34], C. X. Liu[1], F. Liu[1], F. H. Liu[53], Feng Liu[6], G. M. Liu[56,j], H. Liu[38,k,l], H. B. Liu[15], H. H. Liu[1], H. M. Liu[1,64], Huihui Liu[21], J. B. Liu[72,58], J. Y. Liu[1,64], K. Liu[38,k,l], K. Y. Liu[40], Ke Liu[22], L. Liu[72,58], L. C. Liu[43], Lu Liu[43], M. H. Liu[12,g], P. L. Liu[1], Q. Liu[64], S. B. Liu[72,58], T. Liu[12,g], W. K. Liu[43], W. M. Liu[72,58], X. Liu[38,k,l], X. Liu[39], Y. Liu[81], Y. Liu[38,k,l], Y. B. Liu[43], Z. A. Liu[1,58,64], Z. D. Liu[9], Z. Q. Liu[50], X. C. Lou[1,58,64], F. X. Lu[59], H. J. Lu[23], J. G. Lu[1,58], X. L. Lu[1], Y. Lu[7], Y. P. Lu[1,58], Z. H. Lu[1,64], C. L. Luo[41], J. R. Luo[59], M. X. Luo[80], T. Luo[12,g], X. L. Luo[1,58], X. R. Lyu[64], Y. F. Lyu[43], F. C. Ma[40], H. Ma[79], H. L. Ma[1], J. L. Ma[1,64], L. L. Ma[50], L. R. Ma[67], M. M. Ma[1,64], Q. M. Ma[1], R. Q. Ma[1,64], T. Ma[72,58], X. T. Ma[1,64], X. Y. Ma[1,58], Y. M. Ma[31], F. E. Maas[18], I. MacKay[70], M. Maggiora[75A,75C], S. Malde[70], Y. J. Mao[46,h], Z. P. Mao[1], S. Marcello[75A,75C], Z. X. Meng[67], J. G. Messchendorp[13,65], G. Mezzadri[29A], H. Miao[1,64], T. J. Min[42], R. E. Mitchell[27], X. H. Mo[1,58,64], B. Moses[27], N. Yu. Muchnoi[4,c], J. Muskalla[35], Y. Nefedov[36], F. Nerling[18,e], L. S. Nie[20], I. B. Nikolaev[4,c], Z. Ning[1,58], S. Nisar[11,m], Q. L. Niu[38,k,l], W. D. Niu[55], Y. Niu [50], S. L. Olsen[64], S. L. Olsen[10,64], Q. Ouyang[1,58,64], S. Pacetti[28B,28C], X. Pan[55], Y. Pan[57], A. Pathak[34], Y. P. Pei[72,58], M. Pelizaeus[3], H. P. Peng[72,58], Y. Y. Peng[38,k,l], K. Peters[13,e], J. L. Ping[41], R. G. Ping[1,64], S. Plura[35], V. Prasad[33], F. Z. Qi[1], H. Qi[72,58], H. R. Qi[61], M. Qi[42], T. Y. Qi[12,g], S. Qian[1,58], W. B. Qian[64], C. F. Qiao[64], X. K. Qiao[81], J. J. Qin[73], L. Q. Qin[14], L. Y. Qin[72,58], X. P. Qin[12,g], X. S. Qin[50], Z. H. Qin[1,58], J. F. Qiu[1], Z. H. Qu[73], C. F. Redmer[35], K. J. Ren[39], A. Rivetti[75C], M. Rolo[75C], G. Rong[1,64], Ch. Rosner[18], M. Q. Ruan[1,58], S. N. Ruan[43], N. Salone[44], A. Sarantsev[36,d], Y. Schelhaas[35], K. Schoenning[76], M. Scodeggio[29A], K. Y. Shan[12,g], W. Shan[24], X. Y. Shan[72,58], Z. J. Shang[38,k,l], J. F. Shangguan[16], L. G. Shao[1,64], M. Shao[72,58], C. P. Shen[12,g], H. F. Shen[1,8], W. H. Shen[64],

X. Y. Shen[1,64], B. A. Shi[64], H. Shi[72,58], H. C. Shi[72,58], J. L. Shi[12,g], J. Y. Shi[1], Q. Q. Shi[55], S. Y. Shi[73], X. Shi[1,58], J. J. Song[19], T. Z. Song[59], W. M. Song[34,1], Y. J. Song[12,g], Y. X. Song[46,h,n], S. Sosio[75A,75C], S. Spataro[75A,75C], F. Stieler[35], S. S Su[40], Y. J. Su[64], G. B. Sun[77], G. X. Sun[1], H. Sun[64], H. K. Sun[1], J. F. Sun[19], K. Sun[61], L. Sun[77], S. S. Sun[1,64], T. Sun[51,f], W. Y. Sun[34], Y. Sun[9], Y. J. Sun[72,58], Y. Z. Sun[1], Z. Q. Sun[1,64], Z. T. Sun[50], C. J. Tang[54], G. Y. Tang[1], J. Tang[59], M. Tang[72,58], Y. A. Tang[77], L. Y. Tao[73], Q. T. Tao[25,i], M. Tat[70], J. X. Teng[72,58], V. Thoren[76], W. H. Tian[59], Y. Tian[31,64], Z. F. Tian[77], I. Uman[62B], Y. Wan[55], S. J. Wang [50], B. Wang[1], B. L. Wang[64], Bo Wang[72,58], D. Y. Wang[46,h], F. Wang[73], H. J. Wang[38,k,l], J. J. Wang[77], J. P. Wang [50], K. Wang[1,58], L. L. Wang[1], M. Wang[50], N. Y. Wang[64], S. Wang[38,k,l], S. Wang[12,g], T. Wang[12,g], T. J. Wang[43], W. Wang[73], W. Wang[59], W. P. Wang[35,58,72,o], X. Wang[46,h], X. F. Wang[38,k,l], X. J. Wang[39], X. L. Wang[12,g], X. N. Wang[1], Y. Wang[61], Y. D. Wang[45], Y. F. Wang[1,58,64], Y. L. Wang[19], Y. N. Wang[45], Y. Q. Wang[1], Yaqian Wang[17], Yi Wang[61], Z. Wang[1,58], Z. L. Wang[73], Z. Y. Wang[1,64], Ziyi Wang[64], D. H. Wei[14], F. Weidner[69], S. P. Wen[1], Y. R. Wen[39], U. Wiedner[3], G. Wilkinson[70], M. Wolke[76], L. Wollenberg[3], C. Wu[39], J. F. Wu[1,8], L. H. Wu[1], L. J. Wu[1,64], X. Wu[12,g], X. H. Wu[34], Y. Wu[72,58], Y. H. Wu[55], Y. J. Wu[31], Z. Wu[1,58], L. Xia[72,58], X. M. Xian[39], B. H. Xiang[1,64], T. Xiang[46,h], D. Xiao[38,k,l], G. Y. Xiao[42], S. Y. Xiao[1], Y. L. Xiao[12,g], Z. J. Xiao[41], C. Xie[42], X. H. Xie[46,h], Y. Xie[50], Y. G. Xie[1,58], Y. H. Xie[6], Z. P. Xie[72,58], T. Y. Xing[1,64], C. F. Xu[1,64], C. J. Xu[59], G. F. Xu[1], H. Y. Xu[67,2,p], M. Xu[72,58], Q. J. Xu[16], Q. N. Xu[30], W. Xu[1], W. L. Xu[67], X. P. Xu[55], Y. Xu[40], Y. C. Xu[78], Z. S. Xu[64], F. Yan[12,g], L. Yan[12,g], W. B. Yan[72,58], W. C. Yan[81], X. Q. Yan[1,64], H. J. Yang[51,f], H. L. Yang[34], H. X. Yang[1], T. Yang[1], Y. Yang[12,g], Y. F. Yang[1,64], Y. F. Yang[43], Y. X. Yang[1,64], Z. W. Yang[38,k,l], Z. P. Yao[50], M. Ye[1,58], M. H. Ye[8], J. H. Yin[1], Junhao Yin[43], Z. Y. You[59], B. X. Yu[1,58,64], C. X. Yu[43], G. Yu[1,64], J. S. Yu[25,i], M. C. Yu[40], T. Yu[73], X. D. Yu[46,h], Y. C. Yu[81], C. Z. Yuan[1,64], J. Yuan[34], J. Yuan[45], L. Yuan[2], S. C. Yuan[1,64], Y. Yuan[1,64], Z. Y. Yuan[59], C. X. Yue[39], A. A. Zafar[74], F. R. Zeng[50], S. H. Zeng[63A,63B,63C,63D], X. Zeng[12,g], Y. Zeng[25,i], Y. J. Zeng[59], Y. J. Zeng[1,64], X. Y. Zhai[34], Y. C. Zhai[50], Y. H. Zhan[59], A. Q. Zhang[1,64], B. L. Zhang[1,64], B. X. Zhang[1], D. H. Zhang[43], G. Y. Zhang[19], H. Zhang[81], H. Zhang[72,58], H. C. Zhang[1,58,64], H. H. Zhang[34], H. H. Zhang[59], H. Q. Zhang[1,58,64], H. R. Zhang[72,58], H. Y. Zhang[1,58], J. Zhang[59], J. Zhang[81], J. J. Zhang[52], J. L. Zhang[20], J. Q. Zhang[41], J. S. Zhang[12,g], J. W. Zhang[1,58,64], J. X. Zhang[38,k,l], J. Y. Zhang[1], J. Z. Zhang[1,64], Jianyu Zhang[64], L. M. Zhang[61], Lei Zhang[42], P. Zhang[1,64], Q. Y. Zhang[34], R. Y. Zhang[38,k,l], S. H. Zhang[1,64], Shulei Zhang[25,i], X. M. Zhang[1], X. Y Zhang[40], X. Y. Zhang[50], Y. Zhang[1], Y. Zhang[73], Y. T. Zhang[81], Y. H. Zhang[1,58], Y. M. Zhang[39], Yan Zhang[72,58], Z. D. Zhang[1], Z. H. Zhang[1], Z. L. Zhang[34], Z. Y. Zhang[77], Z. Y. Zhang[43], Z. Z. Zhang[45], G. Zhao[1], J. Y. Zhao[1,64], J. Z. Zhao[1,58], L. Zhao[1], Lei Zhao[72,58], M. G. Zhao[43], N. Zhao[79], R. P. Zhao[64], S. J. Zhao[81], Y. B. Zhao[1,58], Y. X. Zhao[31,64], Z. G. Zhao[72,58], A. Zhemchugov[36,b], B. Zheng[73], B. M. Zheng[34], J. P. Zheng[1,58], W. J. Zheng[1,64], Y. H. Zheng[64], B. Zhong[41], X. Zhong[59], H. Zhou[50], J. Y. Zhou[34], L. P. Zhou[1,64], S. Zhou[6], X. Zhou[77], X. K. Zhou[6], X. R. Zhou[72,58], X. Y. Zhou[39], Y. Z. Zhou[12,g], Z. C. Zhou[20], A. N. Zhu[64], J. Zhu[43], K. Zhu[1], K. J. Zhu[1,58,64], K. S. Zhu[12,g], L. Zhu[34], L. X. Zhu[64], S. H. Zhu[71], T. J. Zhu[12,g], W. D. Zhu[41], Y. C. Zhu[72,58], Z. A. Zhu[1,64], J. H. Zou[1], J. Zu[72,58]

(BESIII Collaboration)

[1] *Institute of High Energy Physics, Beijing 100049, People's Republic of China*
[2] *Beihang University, Beijing 100191, People's Republic of China*
[3] *Bochum Ruhr-University, D-44780 Bochum, Germany*
[4] *Budker Institute of Nuclear Physics SB RAS (BINP), Novosibirsk 630090, Russia*
[5] *Carnegie Mellon University, Pittsburgh, Pennsylvania 15213, USA*
[6] *Central China Normal University, Wuhan 430079, People's Republic of China*
[7] *Central South University, Changsha 410083, People's Republic of China*
[8] *China Center of Advanced Science and Technology, Beijing 100190, People's Republic of China*
[9] *China University of Geosciences, Wuhan 430074, People's Republic of China*
[10] *Chung-Ang University, Seoul, 06974, Republic of Korea*
[11] *COMSATS University Islamabad, Lahore Campus, Defence Road, Off Raiwind Road, 54000 Lahore, Pakistan*
[12] *Fudan University, Shanghai 200433, People's Republic of China*
[13] *GSI Helmholtzcentre for Heavy Ion Research GmbH, D-64291 Darmstadt, Germany*
[14] *Guangxi Normal University, Guilin 541004, People's Republic of China*
[15] *Guangxi University, Nanning 530004, People's Republic of China*
[16] *Hangzhou Normal University, Hangzhou 310036, People's Republic of China*

[17] Hebei University, Baoding 071002, People's Republic of China
[18] Helmholtz Institute Mainz, Staudinger Weg 18, D-55099 Mainz, Germany
[19] Henan Normal University, Xinxiang 453007, People's Republic of China
[20] Henan University, Kaifeng 475004, People's Republic of China
[21] Henan University of Science and Technology, Luoyang 471003, People's Republic of China
[22] Henan University of Technology, Zhengzhou 450001, People's Republic of China
[23] Huangshan College, Huangshan 245000, People's Republic of China
[24] Hunan Normal University, Changsha 410081, People's Republic of China
[25] Hunan University, Changsha 410082, People's Republic of China
[26] Indian Institute of Technology Madras, Chennai 600036, India
[27] Indiana University, Bloomington, Indiana 47405, USA
[28] INFN Laboratori Nazionali di Frascati , (A)INFN Laboratori Nazionali di Frascati, I-00044, Frascati, Italy; (B)INFN Sezione di Perugia, I-06100, Perugia, Italy; (C)University of Perugia, I-06100, Perugia, Italy
[29] INFN Sezione di Ferrara, (A)INFN Sezione di Ferrara, I-44122, Ferrara, Italy; (B)University of Ferrara, I-44122, Ferrara, Italy
[30] Inner Mongolia University, Hohhot 010021, People's Republic of China
[31] Institute of Modern Physics, Lanzhou 730000, People's Republic of China
[32] Institute of Physics and Technology, Peace Avenue 54B, Ulaanbaatar 13330, Mongolia
[33] Instituto de Alta Investigación, Universidad de Tarapacá, Casilla 7D, Arica 1000000, Chile
[34] Jilin University, Changchun 130012, People's Republic of China
[35] Johannes Gutenberg University of Mainz, Johann-Joachim-Becher-Weg 45, D-55099 Mainz, Germany
[36] Joint Institute for Nuclear Research, 141980 Dubna, Moscow region, Russia
[37] Justus-Liebig-Universitaet Giessen, II. Physikalisches Institut, Heinrich-Buff-Ring 16, D-35392 Giessen, Germany
[38] Lanzhou University, Lanzhou 730000, People's Republic of China
[39] Liaoning Normal University, Dalian 116029, People's Republic of China
[40] Liaoning University, Shenyang 110036, People's Republic of China
[41] Nanjing Normal University, Nanjing 210023, People's Republic of China
[42] Nanjing University, Nanjing 210093, People's Republic of China
[43] Nankai University, Tianjin 300071, People's Republic of China
[44] National Centre for Nuclear Research, Warsaw 02-093, Poland
[45] North China Electric Power University, Beijing 102206, People's Republic of China
[46] Peking University, Beijing 100871, People's Republic of China
[47] Qufu Normal University, Qufu 273165, People's Republic of China
[48] Renmin University of China, Beijing 100872, People's Republic of China
[49] Shandong Normal University, Jinan 250014, People's Republic of China
[50] Shandong University, Jinan 250100, People's Republic of China
[51] Shanghai Jiao Tong University, Shanghai 200240, People's Republic of China
[52] Shanxi Normal University, Linfen 041004, People's Republic of China
[53] Shanxi University, Taiyuan 030006, People's Republic of China
[54] Sichuan University, Chengdu 610064, People's Republic of China
[55] Soochow University, Suzhou 215006, People's Republic of China
[56] South China Normal University, Guangzhou 510006, People's Republic of China
[57] Southeast University, Nanjing 211100, People's Republic of China
[58] State Key Laboratory of Particle Detection and Electronics, Beijing 100049, Hefei 230026, People's Republic of China
[59] Sun Yat-Sen University, Guangzhou 510275, People's Republic of China
[60] Suranaree University of Technology, University Avenue 111, Nakhon Ratchasima 30000, Thailand
[61] Tsinghua University, Beijing 100084, People's Republic of China
[62] Turkish Accelerator Center Particle Factory Group, (A)Istinye University, 34010, Istanbul, Turkey; (B)Near East University, Nicosia, North Cyprus, 99138, Mersin 10, Turkey
[63] University of Bristol, (A)H H Wills Physics Laboratory; (B)Tyndall Avenue; (C)Bristol; (D)BS8 1TL

[64] University of Chinese Academy of Sciences, Beijing 100049, People's Republic of China
[65] University of Groningen, NL-9747 AA Groningen, The Netherlands
[66] University of Hawaii, Honolulu, Hawaii 96822, USA
[67] University of Jinan, Jinan 250022, People's Republic of China
[68] University of Manchester, Oxford Road, Manchester, M13 9PL, United Kingdom
[69] University of Muenster, Wilhelm-Klemm-Strasse 9, 48149 Muenster, Germany
[70] University of Oxford, Keble Road, Oxford OX13RH, United Kingdom
[71] University of Science and Technology Liaoning, Anshan 114051, People's Republic of China
[72] University of Science and Technology of China, Hefei 230026, People's Republic of China
[73] University of South China, Hengyang 421001, People's Republic of China
[74] University of the Punjab, Lahore-54590, Pakistan
[75] University of Turin and INFN, (A)University of Turin, I-10125, Turin, Italy; (B)University of Eastern Piedmont, I-15121, Alessandria, Italy; (C)INFN, I-10125, Turin, Italy
[76] Uppsala University, Box 516, SE-75120 Uppsala, Sweden
[77] Wuhan University, Wuhan 430072, People's Republic of China
[78] Yantai University, Yantai 264005, People's Republic of China
[79] Yunnan University, Kunming 650500, People's Republic of China
[80] Zhejiang University, Hangzhou 310027, People's Republic of China
[81] Zhengzhou University, Zhengzhou 450001, People's Republic of China

[a] Deceased
[b] Also at the Moscow Institute of Physics and Technology, Moscow 141700, Russia
[c] Also at the Novosibirsk State University, Novosibirsk, 630090, Russia
[d] Also at the NRC "Kurchatov Institute", PNPI, 188300, Gatchina, Russia
[e] Also at Goethe University Frankfurt, 60323 Frankfurt am Main, Germany
[f] Also at Key Laboratory for Particle Physics, Astrophysics and Cosmology, Ministry of Education; Shanghai Key Laboratory for Particle Physics and Cosmology; Institute of Nuclear and Particle Physics, Shanghai 200240, People's Republic of China
[g] Also at Key Laboratory of Nuclear Physics and Ion-beam Application (MOE) and Institute of Modern Physics, Fudan University, Shanghai 200443, People's Republic of China
[h] Also at State Key Laboratory of Nuclear Physics and Technology, Peking University, Beijing 100871, People's Republic of China
[i] Also at School of Physics and Electronics, Hunan University, Changsha 410082, China
[j] Also at Guangdong Provincial Key Laboratory of Nuclear Science, Institute of Quantum Matter, South China Normal University, Guangzhou 510006, China
[k] Also at MOE Frontiers Science Center for Rare Isotopes, Lanzhou University, Lanzhou 730000, People's Republic of China
[l] Also at Lanzhou Center for Theoretical Physics, Lanzhou University, Lanzhou 730000, People's Republic of China
[m] Also at the Department of Mathematical Sciences, IBA, Karachi 75270, Pakistan
[n] Also at Ecole Polytechnique Federale de Lausanne (EPFL), CH-1015 Lausanne, Switzerland
[o] Also at Helmholtz Institute Mainz, Staudinger Weg 18, D-55099 Mainz, Germany
[p] Also at School of Physics, Beihang University, Beijing 100191 , China

The $e^+e^- \to D_s^+ D_{s1}(2536)^-$ and $e^+e^- \to D_s^+ D_{s2}^*(2573)^-$ processes are studied using data samples collected with the BESIII detector at center-of-mass energies from 4.530 to 4.946 GeV. The absolute branching fractions of $D_{s1}(2536)^- \to \bar{D}^{*0}K^-$ and $D_{s2}^*(2573)^- \to \bar{D}^0 K^-$ are measured for the first time to be $(35.9\pm4.8\pm3.5)\%$ and $(37.4\pm3.1\pm4.6)\%$, respectively. The measurements are in tension with predictions based on the assumption that the $D_{s1}(2536)$ and $D_{s2}^*(2573)$ are dominated by a bare $c\bar{s}$ component. The $e^+e^- \to D_s^+ D_{s1}(2536)^-$ and $e^+e^- \to D_s^+ D_{s2}^*(2573)^-$ cross sections are measured, and a resonant structure at around 4.6 GeV with a width of 50 MeV is observed for the first time with a statistical significance of 15σ in the $e^+e^- \to D_s^+ D_{s2}^*(2573)^-$ process. It could be the $Y(4626)$ found by the Belle collaboration in the $D_s^+ D_{s1}(2536)^-$ final state, since they have similar masses and widths. There is also evidence for a structure at around 4.75 GeV in both processes.

The D_s mesons are bound states of $c\bar{s}$ quarks. Four P-wave $c\bar{s}$ states with $J^P = 0^+$ (D_{s0}^*), 1^+ (D_{s1}), 1^+ (D'_{s1}), and 2^+ (D_{s2}^*) are predicted in the conventional quark model [1], and the four experimentally observed states $D_{s0}^*(2317)$, $D_{s1}(2460)$, $D_{s1}(2536)$, and $D_{s2}^*(2573)$ are assigned to them, respectively. Recently, authors of Ref. [2] developed a coupled-channel framework which considers the quark-pair-creation mechanism and $D^{(*)}K$ interactions to investigate the inner structures of these states. The framework explains the lower measured masses of $D_{s0}^*(2317)$ [3] and $D_{s1}(2460)$ [4] compared with those predicted by the conventional quark model and infers that $(98.2^{+0.1}_{-0.2})\%$ and $(95.9^{+1.0}_{-1.5})\%$ of the contents of the $D_{s1}(2536)$ and $D_{s2}^*(2573)$, respectively, are bare $c\bar{s}$ cores [2]. At the heavy quark limit and regarding $D_{s1}(2536)$ and $D_{s2}^*(2573)$ as being dominated by a bare $c\bar{s}$ core, authors of Ref. [1] predict the absolute branching fractions of $D_{s1}(2536) \to D^*K$ and $D_{s2}^*(2573) \to DK$ to be 100% and 93.4%, respectively. Experimental measurements of $D_{s1}(2536) \to D^*K$ and $D_{s2}^*(2573) \to DK$ play an important role in understanding the inner structure of these P-wave charmed-strange mesons.

Effective Field Theory [5–7] and Quantum Chromodynamics-inspired potential models [8–11] predict six vector charmonium states with masses between 4.0 and 4.8 GeV/c^2: $\psi(3^3S_1)$, $\psi(2^3D_1)$, $\psi(4^3S_1)$, $\psi(3^3D_1)$, $\psi(5^3S_1)$, and $\psi(4^3D_1)$. The first three states are usually assigned as $\psi(4040)$, $\psi(4160)$, and $\psi(4415)$, respectively. The unclassified $\psi(3^3D_1)$, $\psi(5^3S_1)$, and $\psi(4^3D_1)$ states are expected to have masses above 4.45 GeV/c^2. However, the $Y(4500)$ [12], $Y(4660)$ [13], $Y(4710)$ [14], and $Y(4790)$ [15] are observed in this mass region, which makes the assignment of these states very uncertain. The $Y(4660)$ is observed through initial state radiation (ISR) in $e^+e^- \to \pi^+\pi^-\psi(2S)$ [13], and the $\pi^+\pi^-$ invariant mass tends to accumulate at the nominal mass of $f_0(980)$, which has an $s\bar{s}$ component [13]; the $Y(4500)$ and $Y(4710)$ are observed in $e^+e^- \to K^+K^-J/\psi$ [12, 14] and the $Y(4790)$ in $e^+e^- \to D_s^{*+}D_s^{*-}$ [15], where K and D_s^* have s components also. These measurements indicate that these four states have both $s\bar{s}$ and $c\bar{c}$ components and may decay into a charmed-strange meson pair. Therefore, the search for possible Y states in $c\bar{s}$ and $\bar{c}s$ meson pairs provides an opportunity to investigate these unclassified Y states. Evidence for $Y(4626)$ in $e^+e^- \to D_s^+D_{s1}(2536)^-$ (charge conjugated processes and particles are always implied in the following) [16] and evidence for a $Y(4620)$ state in $e^+e^- \to D_s^+D_{s2}^*(2573)^-$ [17] are reported by the Belle collaboration in ISR processes with large uncertainties. Improved measurements at BESIII and other experiments are needed to draw more solid conclusions on these states.

In this Letter, the $e^+e^- \to D_s^+D_{s1}(2536)^-$ and $D_s^+D_{s2}^*(2573)^-$ processes are investigated with $D_{s1}(2536)^-$ and $D_{s2}^*(2573)^-$ decaying both inclusively (inclusive analysis) and to $\bar{D}^{*0}K^-$ and $\bar{D}^0K^-$ (exclusive analysis). The absolute branching fractions of $D_{s1}(2536)^- \to \bar{D}^{*0}K^-$ and $D_{s2}^*(2573)^- \to \bar{D}^0K^-$ are measured by comparing the cross sections of inclusive and exclusive processes, and possible Y states are searched for in the exclusive cross sections.

The BESIII detector is described in detail in Refs. [18, 19]. The experimental data samples used in this Letter are taken at center-of-mass energies ($\sqrt{s}$) ranging from 4.530 to 4.946 GeV with 15 energy points [20, 21] corresponding in total to an integrated luminosity of 6.60 fb^{-1} [21, 22]; the details of the data samples are shown in the supplemental material. Since the cross sections of some background processes are not measured for data samples with $\sqrt{s} < 4.6$ GeV and $\sqrt{s} > 4.7$ GeV, only data samples with $4.6 \leq \sqrt{s} < 4.74$ GeV (excluding $\sqrt{s} = 4.610$ GeV due to low statistics) are used for the absolute branching fraction measurements. Cross sections of the exclusive processes at all energy points are measured. Simulated samples, which are used to estimate the background and to determine the detection efficiencies and ISR correction factors, are produced with GEANT4-based [23] Monte Carlo (MC) software, which includes the geometric description of the BESIII detector and its response.

The $e^+e^- \to D_s^+D_{s1}(2536)^-$ process is simulated with the AngSam model [24, 25], using an angular distribution described by $1 + \alpha\cos^2\theta$, where θ is the polar angle of D_s^+ in the e^+e^- rest frame, and $\alpha = -0.65 \pm 0.22$ is measured in this work. The $D_{s1}(2536)^- \to \bar{D}^{*0}K^-$ decay is simulated with the VVS_PWAVE model, which describes the decay of a vector particle to a vector and a scalar [24, 25], and the fraction of S-wave and D-wave is fixed according to the Belle measurement [26]. The $e^+e^- \to D_s^+D_{s2}^*(2573)^-$ process is generated via D-wave with $D_{s2}^*(2573)^-$ decaying to $\bar{D}^0K^-$ via D-wave. The $D_s^+ \to K^-K^+\pi^+$ decay is simulated with the D_Dalitz model [24, 25], and the $K_S^0 \to \pi^+\pi^-$ and $D_s^+ \to K_S^0K^+$ decays are simulated with a phase space model [24, 25]. Beam energy spread and ISR are considered with the generator KKMC [27, 28].

In the inclusive measurement, a D_s^+ is reconstructed with the decay of $D_s^+ \to K^-K^+\pi^+$. The selection criteria for charged tracks are described in Ref. [29]. The tracks used to reconstruct D_s^+ are required to originate from a common vertex, and the χ^2 of the vertex fit ($\chi^2_{\rm VF}$) [30] is required to satisfy $\chi^2_{\rm VF} < 100$. Only decays containing the intermediate states ϕ or $\bar{K}^{*0}$ in $D_s^+ \to K^-K^+\pi^+$ are used to select D_s^+ candidates. The invariant masses of K^+K^- ($M(K^+K^-)$) or $K^-\pi^+$ ($M(K^-\pi^+)$) are required to satisfy $1.004 < M(K^+K^-) < 1.034$ GeV/c^2 with a helicity angle of K^+ in the K^+K^- helicity frame satisfying $|\cos\theta_{K^+/K^+K^-}| > 0.4$, or $0.832 < M(K^-\pi^+) < 0.928$ GeV/c^2 with $|\cos\theta_{\pi^+/K^-\pi^+}| > 0.52$. The invariant mass of $K^-K^+\pi^+$ ($M(K^-K^+\pi^+)$) is constrained to the known D_s^+ mass

$m_{D_s^+}$ [31] using a one-constraint kinematic fit to improve the resolution of the D_s^+ recoiling mass, $RM(D_s^+)$.

The yields of $D_{s1}(2536)^-$ and $D_{s2}^*(2573)^-$ events are determined by a two-dimensional (2D) extended unbinned likelihood fit to $M(K^-K^+\pi^+)$ versus $RM(D_s^+)$. Distributions of $RM(D_s^+)$ versus $M(K^-K^+\pi^+)$ from data and the projection of the 2D fit in $RM(D_s^+)$ at $\sqrt{s} = 4.680$ GeV are shown in Figs. 1(a) and 1(b), respectively. The details of the fit methods in inclusive and exclusive measurements and numerical results of the cross section calculation are described in the supplemental material. The cross sections are calculated with

$$\sigma^{\rm inc}_{i,j} = \frac{N^{\rm inc}_{i,j}}{\frac{1}{|1-\Pi|^2}(1+\delta)_{i,j}\epsilon^{\rm inc}_{i,j}\mathcal{B}_{K^-K^+\pi^+}\mathcal{L}}, \tag{1}$$

where $\mathcal{B}_{K^-K^+\pi^+}$ is the branching fraction of $D_s^+ \to K^-K^+\pi^+$ [31], $N^{\rm inc}_{i,j}$ is the number of signal events obtained from the 2D fit, $(1+\delta)_{i,j}$ is the ISR correction factor obtained from MC simulation, and $\epsilon^{\rm inc}_{i,j}$ is the detection efficiency for $e^+e^- \to D_s^+D_{s1}(2536)^-$ $(i = 1)$ or $e^+e^- \to D_s^+D_{s2}^*(2573)^-$ $(i = 2)$ in the inclusive cross section measurement at the $j^{\rm th}$ $\sqrt{s}$; $\frac{1}{|1-\Pi|^2}$ and $\mathcal{L}$ are the vacuum polarization factor and integrated luminosity at the corresponding $\sqrt{s}$, respectively.

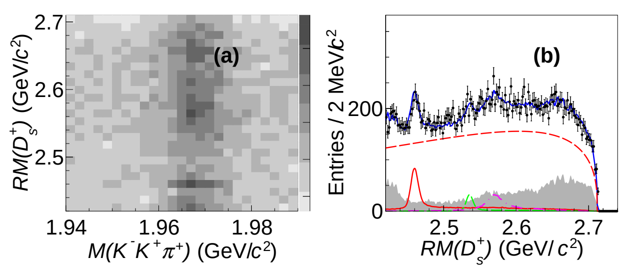

FIG. 1. Distribution of (a) $RM(D_s^+)$ versus $M(K^-K^+\pi^+)$ from data and (b) projection of the 2D fit in $RM(D_s^+)$ in the inclusive analysis at $\sqrt{s} = 4.680$ GeV. Here, the dots with error bars are data, the gray histogram is background from processes involving an excited D_s or D meson, the red dashed line is an ARGUS function [32], the blue solid line is the total fit, and the red solid, green dashed, and purple dash-dotted lines are MC shapes of $D_{s1}(2460)^-$, $D_{s1}(2536)^-$, and $D_{s2}^*(2573)^-$ signals, respectively.

In the exclusive measurement, a D_s^+ is reconstructed with the decay of $D_s^+ \to K^-K^+\pi^+$ or $D_s^+ \to K_S^0(\to \pi^+\pi^-)K^+$ and a K^- is selected from the charged tracks not forming the D_s^+. The selection criteria for K_S^0 are described in Refs. [29, 30]. The tracks used to reconstruct D_s^+, including the virtual track of K_S^0 from a secondary vertex fit [30], are also required to originate from a common vertex with $\chi^2_{\rm VF} < 100$. In addition to the selection criteria used in the inclusive analysis, the invariant mass of $K^-K^+\pi^+$ or $K_S^0K^+$ $(M(K_S^0K^+))$ must satisfy $|M(K^-K^+\pi^+/K_S^0K^+)-m_{D_s^+}| < 8$ MeV/c^2. To select $D_{s2}^*(2573)^- \to \bar{D}^0K^-$ and $D_{s1}(2536)^- \to \bar{D}^{*0}K^-$, the recoiling mass of $D_s^+K^-$ $(RM(D_s^+K^-))$ must satisfy the following requirements: for the $e^+e^- \to D_s^+D_{s1}(2536)^-$ process, $|RM(D_s^+K^-)-m_{\bar{D}^{*0}}|$ should be less than 9 MeV/c^2 for $D_s^+ \to K^-K^+\pi^+$ and 7 MeV/c^2 for $D_s^+ \to K_S^0K^+$; for the $e^+e^- \to D_s^+D_{s2}^*(2573)^-$ process, $|RM(D_s^+K^-) - m_{\bar{D}^0}|$ should be less than 11 MeV/c^2 for $D_s^+ \to K^-K^+\pi^+$ and 9 MeV/c^2 for $D_s^+ \to K_S^0K^+$. Here, $m_{\bar{D}^{*0}}$ and $m_{\bar{D}^0}$ are the known $\bar{D}^{*0}$ and $\bar{D}^0$ masses, respectively [31]. For the selected entries, $M(K^-K^+\pi^+/K_S^0K^+)$ is constrained to $m_{D_s^+}$, $RM(D_s^+K^-)$ is constrained to $m_{\bar{D}^0}$ or $m_{\bar{D}^{*0}}$, and the total four-momentum is constrained to that of the initial e^+e^- system via a kinematic fit.

For data samples with $\sqrt{s} \geq 4.6$ GeV, the yields of $D_{s1}(2536)^-$ and $D_{s2}^*(2573)^-$ events are determined by extended unbinned likelihood fits to the corresponding $RM(D_s^+)$ distributions, while for data samples with $\sqrt{s} < 4.6$ GeV, due to the low number of events, the counting method described in Refs. [33, 34] is used. The fit results of $RM(D_s^+)$ for $D_{s1}(2536)^-$ and $D_{s2}^*(2573)^-$ at $\sqrt{s} = 4.680$ GeV are shown in Figs. 2(a) and 2(b), respectively. The cross sections are calculated with

$$\sigma^{\rm exc}_{i,j} = \frac{N^{\rm exc}_{i,j}}{\frac{1}{|1-\Pi|^2}(1+\delta)_{i,j}(\epsilon\mathcal{B})_{i,j}\mathcal{L}}, \tag{2}$$

where $N^{\rm exc}_{i,j}$ is the number of signal events obtained from the fit and $(\epsilon\mathcal{B})_{i,j} = (\epsilon^{\rm exc}_{K^-K^+\pi^+,i,j}\mathcal{B}_{K^-K^+\pi^+} + \epsilon^{\rm exc}_{K_S^0K^+,i,j}\mathcal{B}_{K_S^0K^+})$. Here, $\mathcal{B}_{K_S^0K^+} = \mathcal{B}(D_s^+ \to K_S^0K^+)\mathcal{B}(K_S^0 \to \pi^+\pi^-)$ [31] is the product of the branching fractions of $D_s^+ \to K_S^0K^+$ and $K_S^0 \to \pi^+\pi^-$, $\epsilon^{\rm exc}_{K^-K^+\pi^+,i,j}$ and $\epsilon^{\rm exc}_{K_S^0K^+,i,j}$ are the detection efficiencies for the signal processes with $D_s^+ \to K^-K^+\pi^+$ and $D_s^+ \to K_S^0(\to \pi^+\pi^-)K^+$, respectively. The measured cross sections of $e^+e^- \to D_s^+D_{s1}(2536)^-$ and $e^+e^- \to D_s^+D_{s2}^*(2573)^-$ with the inclusive and exclusive methods are shown in Figs. 3(a) and 3(b), respectively.

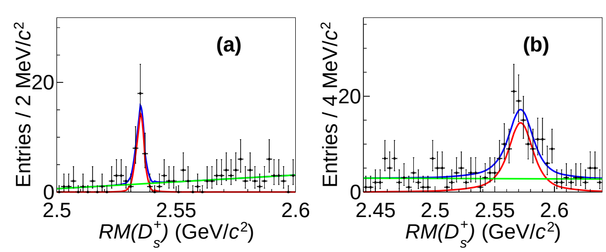

FIG. 2. Fit results of $RM(D_s^+)$ for (a) $D_{s1}(2536)^-$ and (b) $D_{s2}^*(2573)^-$ in the exclusive analysis at $\sqrt{s} = 4.680$ GeV. Here, the dots with error bars are data, the blue, red, and green solid lines are the total fit, signal shape, and background shape, respectively.

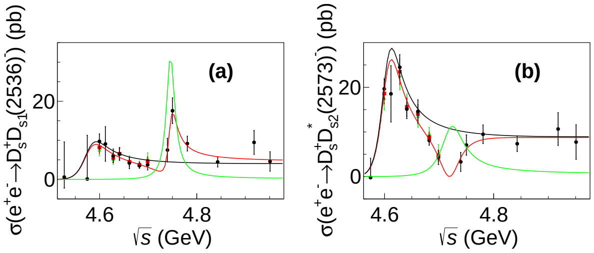

FIG. 3. Cross sections of (a) $e^+e^- \to D_s^+ D_{s1}(2536)^-$ with $D_{s1}(2536)^- \to \bar{D}^{*0}K^-$ and (b) $e^+e^- \to D_s^+ D_{s2}^*(2573)^-$ with $D_{s2}^*(2573)^- \to \bar{D}^0 K^-$. The black dots, red squares, and green triangles with error bars are measured exclusive cross sections, inclusive cross section from likelihood fit multiplied by the absolute branching fraction, and measured inclusive cross section multiplied by the absolute branching fraction, respectively. The red, black, and green solid lines are results of total fit, BW_0, and BW_1, respectively. The uncertainties are statistical only.

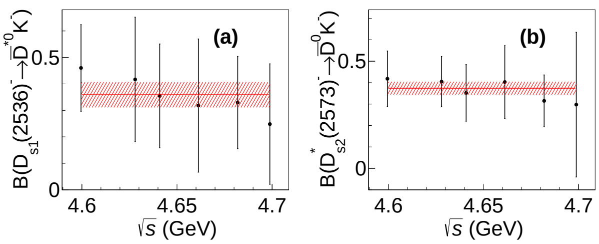

FIG. 4. The absolute branching fractions of (a) $D_{s1}(2536)^- \to \bar{D}^{*0}K^-$ and (b) $D_{s2}^*(2573)^- \to \bar{D}^0K^-$. The black dots with error bars are absolute branching fractions calculated at each $\sqrt{s}$, where $\mathcal{B}_{i,j} = \sigma_{i,j}^{\rm exc}/\sigma_{i,j}^{\rm inc}$. The red lines represent results calculated by the maximum likelihood fit. The uncertainties are statistical only and are shown with the red shaded bands.

Using the data at the six energy points with both inclusive and exclusive cross sections measured, we determine the absolute branching fractions of the $D_{s1}(2536)^- \to \bar{D}^{*0}K^-$ and $D_{s2}^*(2573)^- \to \bar{D}^0K^-$ with a likelihood fit that maximizes the likelihood function,

$$L_i(\sigma_{i,j}^{\rm inc}, \delta_{i,j}^{\rm inc}, \sigma_{i,j}^{\rm exc}, \delta_{i,j}^{\rm exc}; \sigma_{i,j}, \mathcal{B}_i) = \prod_{j=1}^{6} L_{i,j}^{\rm inc}(\sigma_{i,j}^{\rm inc}, \delta_{i,j}^{\rm inc}; \sigma_{i,j}) L_{i,j}^{\rm exc}(\sigma_{i,j}^{\rm exc}, \delta_{i,j}^{\rm exc}; \sigma_{i,j}, \mathcal{B}_i), \quad (3)$$

where $\delta_{i,j}^{\rm inc}$ and $\delta_{i,j}^{\rm exc}$ are the statistical uncertainties of the measured inclusive and exclusive cross sections, respectively; $\sigma_{i,j}$ is the actual cross section of $e^+e^- \to D_s^+D_{s1}(2536)^-$ or $e^+e^- \to D_s^+D_{s2}^*(2573)^-$; and $\mathcal{B}_i$ is the absolute branching fraction of $D_{s1}(2536)^- \to \bar{D}^{*0}K^-$ ($i = 1$) or $D_{s2}^*(2573)^- \to \bar{D}^0K^-$ ($i = 2$). Since the significances for $e^+e^- \to D_s^+D_{s1}(2536)^-$ ($e^+e^- \to D_s^+D_{s2}^*(2573)^-$) at $\sqrt{s} = 4.66$ (4.66 and 4.7) GeV in both inclusive and exclusive measurements are less than 5σ, $L_{i,j}^{\rm inc,exc}$ at that energy point is a normalized likelihood as a function of $\sigma_{i,j}^{\rm inc,exc}$ which is obtained from the signal yield fits. The likelihood $L_{i,j}^{\rm inc,exc}$ for the other samples with sufficiently high statistics is approximated as a Gaussian function, and details are described in the supplemental material. Figures 4(a) and 4(b) show the fit results of the absolute branching fractions, which are $(35.9 \pm 4.8)\%$ and $(37.4 \pm 3.1)\%$ for $\mathcal{B}(D_{s1}(2536)^- \to \bar{D}^{*0}K^-)$ and $\mathcal{B}(D_{s2}^*(2573)^- \to \bar{D}^0K^-)$, respectively.

To study the resonance structures in the $e^+e^- \to D_s^+D_{s1}(2536)^-$ and $e^+e^- \to D_s^+D_{s2}^*(2573)^-$ processes, least-χ^2 fits to the measured cross sections are performed. The cross sections are described with the coherent sum of two constant-width Breit-Wigner (BW) functions. The fit results are shown in Figs. 3(a) and 3(b) with $\chi^2/\text{ndf} = 4.0/8$ and $6.2/7$, respectively, where ndf is the number of degrees of freedom, and the fit details are described in the supplemental material. By comparing $\Delta\chi^2$ of the fits with and without the corresponding component and accounting for Δndf, the significance is determined. The statistical significances of the first and second resonance structures are 7.2σ and 4.3σ, respectively, in $e^+e^- \to D_s^+D_{s1}(2536)^-$, and 15σ and 2.7σ, respectively, in $e^+e^- \to D_s^+D_{s2}^*(2573)^-$. In both processes, the first resonance structure is around 4.6 GeV with a width of 50 MeV. In $e^+e^- \to D_s^+D_{s1}(2536)^-$, the second one is around 4.75 GeV with a width of 25 MeV, and in $e^+e^- \to D_s^+D_{s2}^*(2573)^-$, around 4.72 GeV with a width of 50 MeV. Continuum contributions are also tested, but the significances are less than 1σ in both processes.

The systematic uncertainties for the measurements of absolute branching fractions related to fits, including signal and background descriptions and fit ranges in the fits of inclusive and exclusive analyses, are described in the supplemental material. The other systematic uncertainties are introduced below.

The systematic uncertainties from the mass window requirement of $M(D_s^+)$ ($RM(D_s^+K^-)$) are estimated by comparing the efficiency difference between data and MC simulation [35] as 3.4% and 5.5% (4.3% and 4.3%), for $D_{s1}(2536)^- \to \bar{D}^{*0}K^-$ and $D_{s2}^*(2573)^- \to \bar{D}^0K^-$, respectively.

The systematic uncertainties from tracking (particle identification, PID) efficiencies for $K^\pm$ and π^+ from D_s^+ are taken as 0.5% (0.5%) and 0.2% (0.4%), respectively [36]. The systematic uncertainty from K_S^0 reconstruction is assigned as 2.3% [37]. Most of these uncertainties cancel in the D_s^+ reconstruction as they appear in both inclusive and exclusive processes. Only those uncertainties not common between the two are considered, and the systematic uncertainties from $D_s^+ \to K^-K^+\pi^+$ and $D_s^+ \to K_S^0K^+$ are added according to their branching fractions. Since the momentum of the bachelor K^- that does not come from D_s^+ decays in the exclusive analysis is very low, the systematic uncertainties of this K^- are estimated with a control sample of $J/\psi \to pK^-\Lambda$ [38] as 1.2% and 0.0% for $D_{s1}(2536)^- \to \bar{D}^{*0}K^-$ and $D^*_{s2}(2573)^- \to \bar{D}^0K^-$, respectively.

The uncertainties of $\mathcal{B}(D_s^+ \to K^-K^+\pi^+)$ and $\mathcal{B}(D_s^+ \to K^0_SK^+)$ are 1.9% and 2.4% [31], respectively. The systematic uncertainty from $\mathcal{B}(D_s^+ \to K^-K^+\pi^+)$ cancels out in the calculation of the absolute branching fractions, but does not cancel in the exclusive cross section measurements.

The fractions of the S-wave and D-wave of the $D_{s1}(2536)^- \to \bar{D}^{*0}K^-$ decay are changed by one standard deviation, and the systematic uncertainty is estimated by the maximum change at $\sqrt{s} = 4.680$ GeV on the exclusive cross section as 0.2%.

The total systematic uncertainties are 9.7% and 12.4% for the two processes, respectively, by assuming all sources to be independent and summing them in quadrature.

Most systematic uncertainty estimations for the exclusive cross section measurements are the same as those described for the absolute branching fraction measurements, including the mass window requirements, $\mathcal{B}(D_s^+ \to K^-K^+\pi^+)$ and $\mathcal{B}(D_s^+ \to K^0_SK^+)$, the fraction of the S-wave and D-wave in the $D_{s1}(2536)^- \to \bar{D}^{*0}K^-$ decay, and tracking and PID efficiencies, where 1.9% is assigned for tracks from D_s^+ for both processes. Systematic uncertainties related to the fit, including the fit range and background shape, are described in the supplemental material. Additional sources of systematic uncertainties unique to the exclusive cross section measurement are described below.

The angular distribution of $e^+e^- \to D_s^+D_{s1}(2536)^-$ is described by $1 + \alpha\cos^2\theta$ with the AngSam model. To estimate the systematic uncertainty from this model, α is changed by one standard deviation and the maximum change at $\sqrt{s}$ =4.680 GeV is taken as the uncertainty of 3.3%. The ISR correction factor and efficiency of the signal process depend on the input cross section in kkmc. We sample the input cross section 500 times at each $\sqrt{s}$ according to its statistical uncertainty, and take the ratio of the standard deviation and the mean value of $\epsilon(1+\delta)$ as the systematic uncertainty. The uncertainty from the luminosity measurement is 1% [21, 22].

The systematic uncertainties introduced above, as well as the total ones are shown in Tables I and II. Tables with all systematic uncertainties are provided in the supplemental material. The systematic uncertainties of the data sample at $\sqrt{s} = 4.600$ GeV are assigned to those of the data samples at $\sqrt{s} = 4.530$ and 4.575 GeV because of low statistics.

In summary, we measure for the first time the absolute branching fractions of $D_{s1}(2536)^- \to \bar{D}^{*0}K^-$ and $D^*_{s2}(2573)^- \to \bar{D}^0K^-$ as $(35.9 \pm 4.8 \pm 3.5)\%$ and $(37.4 \pm 3.1 \pm 4.6)\%$, respectively, where the first uncertainties are statistical and the second systematic. Assuming isospin symmetry and neglecting the phase space differences, we obtain $\mathcal{B}(D_{s1}(2536)^- \to (\bar{D}^*\bar{K})^-) = (71.8 \pm 9.6 \pm 7.0)\%$ and $\mathcal{B}(D^*_{s2}(2573)^- \to (\bar{D}\bar{K})^-) = (74.8 \pm 6.2 \pm 9.2)\%$. $\mathcal{B}(D_{s1}(2536)^- \to (\bar{D}^*\bar{K})^-)$ $(\mathcal{B}(D^*_{s2}(2573)^- \to (\bar{D}\bar{K})^-))$ is more than two (one) standard deviations from the prediction of Refs. [1, 40], about 100% (90%), if $D_{s1}(2536)$ $(D^*_{s2}(2573))$ is predominantely a bare $c\bar{s}$ meson. Our measurements indicate that non-$c\bar{s}$ components may exist in the $D_{s1}(2536)$ and $D^*_{s2}(2573)$ wave functions. The exclusive cross sections of $e^+e^- \to D_s^+D_{s1}(2536)^-$ with $D_{s1}(2536)^- \to \bar{D}^{*0}K^-$ and $e^+e^- \to D_s^+D^*_{s2}(2573)^-$ with $D^*_{s2}(2573)^- \to \bar{D}^0K^-$ are also reported in this Letter. A resonant structure at around 4.6 GeV is observed for the first time in $e^+e^- \to D_s^+D^*_{s2}(2573)^-$, which is consistent with the evidence for the $Y(4620)$ with the same final state reported by the Belle collaboration [17]. A clear enhancement at around 4.6 GeV is also observed in $e^+e^- \to D_s^+D_{s1}(2536)^-$, which could be the $Y(4626)$ state observed by the Belle collaboration [16] in the same final state. Our data may indicate that the same state at around 4.6 GeV decays into both $D_s^+D_{s1}(2536)^-$ and $D_s^+D^*_{s2}(2573)^-$ final states. Evidence for a structure at around 4.75 GeV is observed, which may be the $Y(4710)$ or $Y(4790)$ reported earlier by the BESIII experiment [14, 15].

Acknowledgment

The BESIII Collaboration thanks the staff of BEPCII and the IHEP computing center for their strong support. This work is supported in part by National Key R&D Program of China under Contracts Nos. 2020YFA0406300, 2020YFA0406400, 2023YFA1606000; National Natural Science Foundation of China (NSFC) under Contracts Nos. 11635010, 11735014, 11935015, 11935016, 11935018, 12025502, 12035009, 12035013, 12061131003, 12192260, 12192261, 12192262, 12192263, 12192264, 12192265, 12221005, 12225509, 12235017, 12361141819; the Chinese Academy of Sciences (CAS) Large-Scale Scientific Facility Program; the CAS Center for Excellence in Particle Physics (CCEPP); Joint Large-Scale Scientific Facility Funds of the NSFC and CAS under Contract No. U1832207; 100 Talents Program of CAS; The Institute of Nuclear and Particle Physics (INPAC) and Shanghai Key Laboratory for Particle Physics and Cosmology; German Research Foundation DFG under Contracts Nos. 455635585, FOR5327, GRK 2149; Istituto Nazionale di Fisica Nucleare, Italy; Ministry of Development of Turkey under Contract No. DPT2006K-120470; National Research Foundation of Korea under Contract No. NRF-2022R1A2C1092335; National Science and Technology fund of Mongolia; National Science Research and Innovation Fund (NSRF) via the Program Management Unit for Human Resources & Institutional Development, Research and Innovation of Thailand under Contract No. B16F640076; Polish National Science Centre under Contract No. 2019/35/O/ST2/02907; The Swedish Research Council; U. S. Department of Energy under

TABLE I. Systematic uncertainties (%) in the cross sections for $e^+e^- \to D_s^+ D_{s1}(2536)^-$. "..." represents systematic uncertainties related to fit or common among data samples.

$\sqrt{s}$ (GeV)	4.600	4.610	4.620	4.640	4.660	4.680	4.700	4.740	4.750	4.780	4.840	4.914	4.946
Tracking & PID ($K^\pm$ not from D_s^+)	1.7	1.5	1.4	1.6	1.3	1.2	1.1	0.9	0.9	0.8	0.8	0.8	0.8
ISR	1.4	3.5	3.6	1.9	2.2	1.7	2.0	3.2	1.1	1.0	0.9	0.4	2.3
...	...	...	...	...	...	...	...	...	...	...	...	...	...
Total	9.2	9.2	12.5	10.1	10.0	7.9	8.0	8.3	11.2	9.8	10.3	11.2	15.6

TABLE II. Relative systematic uncertainties (%) in the cross section for $e^+e^- \to D_s^+ D_{s2}^*(2573)^-$. Definition of "..." is the same as in Table I.

$\sqrt{s}$ (GeV)	4.600	4.610	4.620	4.640	4.660	4.680	4.700	4.740	4.750	4.780	4.840	4.914	4.946
Tracking & PID ($K^\pm$ not from D_s^+)	0.1	0.1	0.0	0.0	0.0	0.1	0.1	0.1	0.0	0.1	0.0	0.1	0.1
ISR	1.0	2.7	1.1	1.3	0.8	1.2	2.9	5.3	2.5	0.7	0.6	0.6	1.6
...	...	...	...	...	...	...	...	...	...	...	...	...	...
Total	8.5	10.6	9.7	15.6	9.7	11.9	11.0	9.9	9.3	10.7	15.2	47.0	27.0

Contract No. DE-FG02-05ER41374.

[1] S. Godfrey and K. Moats, Phys. Rev. D **93**, 034035 (2016).
[2] Z. Yang, G. J. Wang, J. J. Wu, M. Oka and S. L. Zhu Phys. Rev. Lett. **128**, 112001 (2022).
[3] B. Aubert *et al.* (BaBar Collaboration), Phys. Rev. Lett. **90**, 242001 (2003).
[4] D. Besson *et al.* (CLEO Collaboration), Phys. Rev. D **68**, 032002 (2003); **75**, 119908(E) (2007).
[5] N. Brambilla, A. Pineda, J. Soto and A. Vairo, Rev. Mod. Phys. **77**, 1423 (2005).
[6] N. Brambilla *et al.*, Eur. Phys. J. C. **71**, 1534 (2011).
[7] N. Brambilla, S. Eidelman, P. Foka, S. Gardner, A. S. Kronfeld, M. G. Alford, R. Alkofer, M. Butenschoen, T. D. Cohen and J. Erdmenger *et al.*, Eur. Phys. J. C **74**, no.10, 2981 (2014).
[8] E. Eichtem, K. Gottfried, T. Kinoshita, K. D. Lane and T. M. Yan, Phys. Rev. D **17**, 3090 (1978).
[9] S. Godfrey and N. Isgur, Phys. Rev. D **32**, 189 (1985).
[10] T. Barnes, S. Godfrey and E. S. Swanson, Phys. Rev. D **72**, 054026 (2005).
[11] Q. Deng, R. H. Ni, Q. Li, and X. H. Zhong, arXiv:2312.10296.
[12] M. Ablikim *et al.* (BESIII Collaboration), Chin. Phys. C. **46**, 111002 (2022).
[13] X. L. Wang *et al.* (Belle Collaboration), Phys. Rev. Lett. **99**, 142002 (2007).
[14] M. Ablikim *et al.* (BESIII Collaboration), Phys. Rev. Lett. **131**, 211902 (2023).
[15] M. Ablikim *et al.* (BESIII Collaboration), Phys. Rev. Lett. **131**, 151903 (2023).
[16] S. Jia *et al.* (Belle Collaboration), Phys. Rev. D **100**, 111103(R) (2019).
[17] S. Jia *et al.* (Belle Collaboration), Phys. Rev. D **101**, 091101(R) (2020).
[18] M. Ablikim *et al.* (BESIII Collaboration), Nucl. Instrum. Meth. A **614**, 345 (2010).
[19] K. X. Huang *et al.*, Nucl. Sci. Tech. **33**, 142 (2022).
[20] M. Ablikim *et al.* (BESIII Collaboration), Chin. Phys. C **40**, 063001 (2016).
[21] M. Ablikim *et al.* (BESIII Collaboration), Chin. Phys. C **46**, 113003 (2022).
[22] M. Ablikim *et al.* (BESIII Collaboration), Chin. Phys. C **46**, 113002 (2022).
[23] S. Agostinelli *et al.* (GEANT4 Collaboration), Nucl. Instrum. Meth. A **506**, 250 (2003).
[24] D. J. Lange, Nucl. Instrum. Meth. A **462**, 152155 (2001).
[25] R. G. Ping, Chin. Phys. C **32**, 599 (2008).
[26] V. Balagura *et al.* (Belle Collaboration), Phys. Rev. D **77**, 032001 (2008).
[27] S. Jadach, B. F. L. Ward and Z. Was, Comput. Phys. Commun. **130**, 260325 (2000).
[28] S. Jadach, B. F. L. Ward and Z. Was, Phys. Rev. D **63**, 113009 (2001).
[29] M. Ablikim *et al.* (BESIII Collaboration), Phys. Rev. D **92**, 092006 (2015).
[30] M. Xu *et al.*, Chin. Phys. C **33**, 428 (2009).
[31] R. L. Workman *et al.* (Particle Data Group), Prog. Theor. Exp. Phys. **2022**, 083C01 (2022) and 2023 update.
[32] H. Albrecht *et al*. [ARGUS Collaboration], Phys. Lett. B. **241**, 278 (1990).
[33] M. Ablikim *et al.* (BESIII Collaboration), Phys. Rev. D **104**, 012001 (2021).
[34] G. J. Feldman and R. D. Cousins, Phys. Rev. D **57**, 3873 (1998).
[35] M. Ablikim *et al.* (BESIII Collaboration), Phys. Rev. D **106**, 052012 (2022).
[36] M. Ablikim *et al.* (BESIII Collaboration), Phys. Rev. Lett. **131**, 151903 (2023).
[37] M. Ablikim *et al.* (BESIII Collaboration), Phys. Rev. Lett. **109**, 042003 (2012).
[38] M. Ablikim *et al.* (BESIII Collaboration), Phys. Rev. Lett. **126**, 092002 (2021).
[39] M. Ablikim *et al.* (BESIII Collaboration), Phys. Rev. D **101**, 112008 (2020).
[40] R. H. Ni, J. J. Wu, and X. H. Zhong, arXiv:2312.04765.

Supplemental Material for "Study of the decay and production properties of $D_{s1}(2536)$ and $D^{*}_{s2}(2573)$"

I. DATA SAMPLES

This analysis is performed based on the data samples collected with the BESIII detector operating at BEPCII. The center-of-mass energies ($\sqrt{s}$) and the corresponding integrated luminosities of these samples ($\mathcal{L}$) are listed in Table I.

TABLE I. The nominal $\sqrt{s}$ (mentioned in the main body of Letter), measured $\sqrt{s}$, and integrated luminosity of data sample ($\mathcal{L}$) used in this Letter [1–3]. For the measured $\sqrt{s}$ and integrated luminosity, the first uncertainty is statistical and the second systematic.

$\sqrt{s}^{\rm nominal}$ (GeV)	Measured $\sqrt{s}$ (MeV)	$\mathcal{L}$ (pb^{-1})
4.530	4527.14±0.11±0.72	112.12±0.04±0.73
4.575	4574.50±0.18±0.70	48.93±0.03±0.32
4.600	4599.53±0.07±0.74	586.9±0.1±3.9
4.610	4611.86±0.12±0.32	103.83±0.05±0.55
4.620	4628.00±0.06±0.32	521.52±0.11±2.76
4.640	4640.91±0.06±0.38	552.41±0.12±2.93
4.660	4661.24±0.06±0.29	529.63±0.12±2.81
4.680	4681.92±0.08±0.29	1669.31±0.21±8.85
4.700	4698.82±0.10±0.39	536.45±0.12±2.84
4.740	4739.70±0.20±0.30	164.27±0.07±0.87
4.750	4750.05±0.12±0.29	367.21±0.10±1.95
4.780	4780.54±0.12±0.33	512.78±0.12±2.72
4.840	4843.07±0.20±0.31	527.29±0.12±2.79
4.914	4918.02±0.34±0.35	208.11±0.02±1.10
4.946	4950.93±0.36±0.44	160.37±0.07±0.85

II. FIT METHODS AND NUMERICAL RESULTS IN INCLUSIVE AND EXCLUSIVE MEASUREMENTS

In the inclusive analysis, the $D_{s1}(2536)^-$ and $D^*_{s2}(2573)^-$ yields are determined by a two-dimensional (2D) extended unbinned likelihood fit of $M(K^-K^+\pi^+)$ and $RM(D_s^+)$. The probability distribution function (PDF) is defined as

$$\text{PDF} = \sum S_{M(K^-K^+\pi^+)} \times S_{RM(D_s^+)} + B_{M(K^-K^+\pi^+)} \times B_{RM(D_s^+)} + B_{\text{Other B.K.G.}}. \tag{1}$$

Here, $S_{M(K^-K^+\pi^+)}$ is the MC shape convolved with a Gaussian function to account for the difference between data sample and MC simulation. The MC shape is obtained from the $e^+e^- \to D_s^+D_{sj}^-$ process, where D_{sj}^- includes $D_{s1}(2460)^-$, $D_{s1}(2536)^-$, and $D^*_{s2}(2573)^-$; the parameters of the Gaussian function are fixed according to the other fit to $M(K^-K^+\pi^+)$ using the MC shape obtained from the $e^+e^- \to D_s^+D_{s1}(2536)^-$ process as the signal shape and a first order Chebychev polynomial function as the background shape. $B_{M(K^-K^+\pi^+)}$ is a first order Chebychev polynomial function describing the D_s^+ background shape, $S_{RM(D_s^+)}$ is the MC shape obtained from the $e^+e^- \to D_s^+D_{sj}^-$ process, and $B_{RM(D_s^+)}$ is an ARGUS function describing the background shape in $RM(D_s^+)$. $B_{\text{Other B.K.G.}}$ includes the MC shapes obtained from the $e^+e^- \to D_s^{*+}D_s^{*-}$, $e^+e^- \to D_s^{*+}D^*_{s0}(2317)^-$, $e^+e^- \to D_s^{*+}D_{s1}(2460)^-$, $e^+e^- \to D_s^{*+}D^*_{s1}(2536)^-$, $e^+e^- \to D_s^+\bar{D}^0K^-$, $e^+e^- \to D_s^+\bar{D}^{*0}K^-$, $e^+e^- \to D_s^{*+}\bar{D}^0K^-$, and $e^+e^- \to D_s^{*+}\bar{D}^{*0}K^-$ processes, where the normalization factors of the former three processes are estimated according to their cross sections reported in Refs. [4–6], and those of the latter three processes are estimated according to their cross sections measured in this work. For the shapes of $M(K^-K^+\pi^+)$ in $B_{\text{Other B.K.G.}}$, we convolve the MC shape with a Gaussian function. The parameters of the Gaussian function are fixed to those used in $S_{M(K^-K^+\pi^+)}$.

In the exclusive analysis, for data samples with $\sqrt{s} \geq 4.6$ GeV, the $D_{s1}(2536)^-$ and $D^*_{s2}(2573)^-$ yields are determined by an extended unbinned likelihood fit of $RM(D_s^+)$. The signal shape is described by the MC shape convolved with a Gaussian function, and the background shape is described by a first-order Chebychev polynomial function. For the $D_{s1}(2536)^-$ signal, the parameters of the Gaussian function are fixed according to the $RM(D_s^+)$ fit of all data samples, and for the $D^*_{s2}(2573)^-$ signal, the parameters of the Gaussian function are free to vary. The fit results in both inclusive and exclusive analyses at $\sqrt{s} = 4.680$ GeV are shown in Fig. 1. The cross sections of $e^+e^- \to D_s^+D_{s1}(2536)^-$ and $e^+e^- \to D_s^+D^*_{s2}(2573)^-$ used in the branching fraction measurements are shown in Tables II and III, respectively. The exclusive cross sections for $e^+e^- \to D_s^+D_{s1}(2536)^-$ and $e^+e^- \to D_s^+D^*_{s2}(2573)^-$ are shown in Tables VI and VII and Tables VIII and IX, respectively.

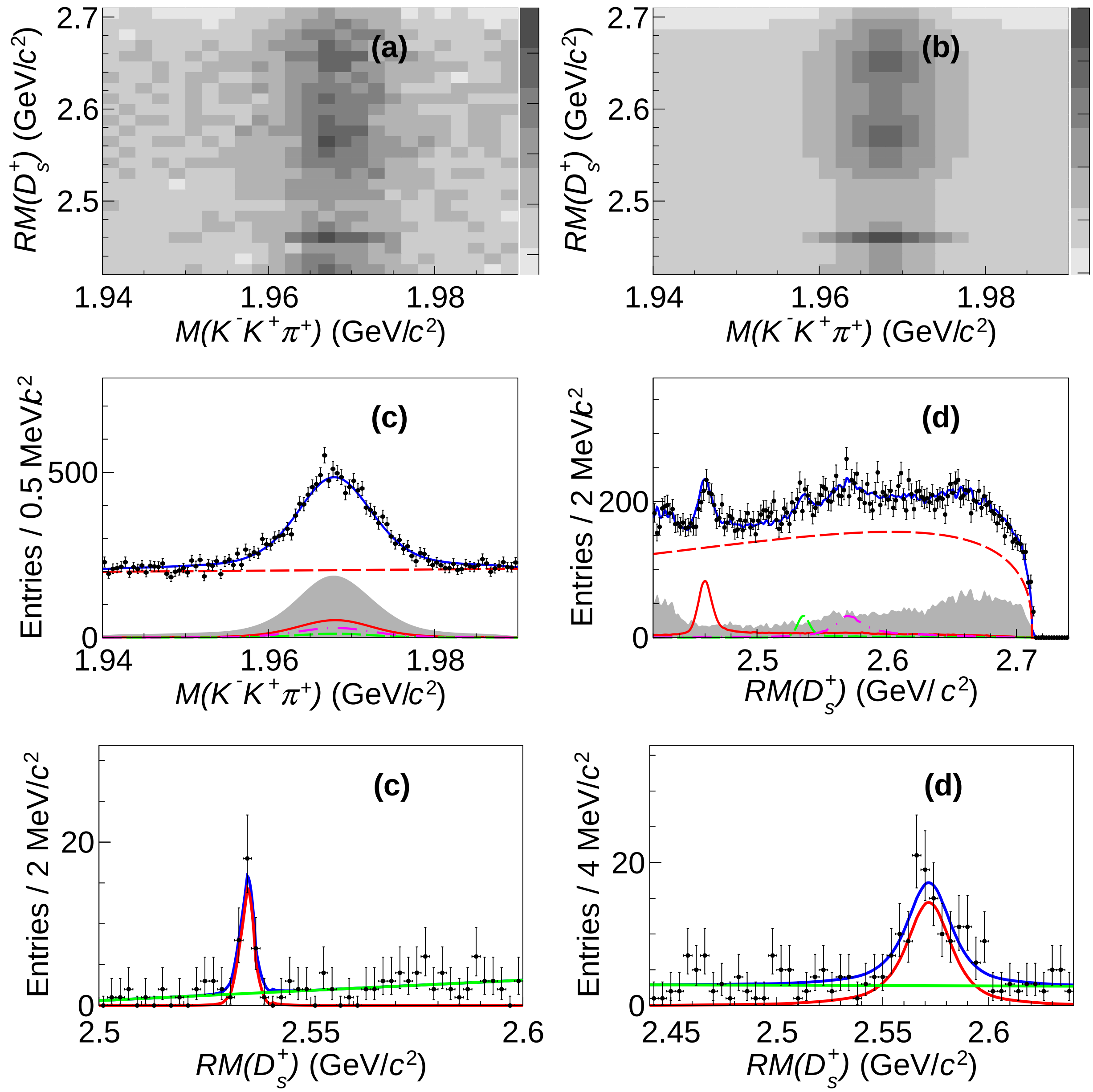

FIG. 1. Top row: Distributions of (a) $RM(D_s^+)$ versus $M(K^-K^+\pi^+)$ in data and (b) total fit results of the 2D fit in the inclusive analysis. Middle row: Projections of the 2D fit in (c) $M(K^-K^+\pi^+)$ and (d) $RM(D_s^+)$ in the inclusive analysis. Here, dots with error bars are data, the gray histograms are $B_{\text{Other B.K.G.}}$, the red dotted lines are $B_{M(K^-K^+\pi^+)} \times B_{RM(D_s^+)}$, the blue solid lines are the total fit, and the red solid, green dashed, purple dash-dotted lines are $S_{M(K^-K^+\pi^+)} \times S_{RM(D_s^+)}$, where $S_{RM(D_s^+)}$ corresponds to the $D_{s1}(2460)^-$, $D_{s1}(2536)^-$, and $D_{s2}^*(2573)^-$ MC signal shapes, respectively. Bottom row: Fit results of (e) $RM(D_s^+)$ for $D_{s1}(2536)^-$ and (f) $D_{s2}^*(2573)^-$ signals in the exclusive analysis. Here, dots with error bars are data, and the blue, red, and green solid lines are the total fit, signal shape, and background shape, respectively.

III. ABSOLUTE BRANCHING FRACTION MEASUREMENT

Formulas of the likelihood $L_{i,j}^{\text{inc,exc}}$ is given as

$$L_{i,j}^{\text{inc}}(\sigma_{i,j}^{\text{inc}}, \delta_{i,j}^{\text{inc}}, \sigma_{i,j}) = \frac{1}{\sqrt{2\pi}\delta_{i,j}^{\text{inc}}} e^{-\frac{(\sigma_{i,j}^{\text{inc}} - \sigma_{i,j})^2}{2(\delta_{i,j}^{\text{inc}})^2}}, \tag{2}$$

TABLE II. The measured cross sections for $e^+e^- \to D_s^+ D_{s1}(2536)^-$. $\sqrt{s}$, $\epsilon_{\rm inc}$, $N_{\rm inc}$, $\epsilon_{\rm exc}(D_s^+ \to K^+K^-\pi^+)$, $\epsilon_{\rm exc}(D_s^+ \to K_S^0 K^+)$, $N_{\rm exc}^{\rm obs}$, $\frac{1}{|1-\Pi|^2}(1+\delta)$, $\sigma^{\rm inc}$, and $\sigma^{\rm exc}$ represent center-of-mass energy, efficiency in the inclusive analysis, number of events observed in the inclusive analysis, efficiency of $D_s^+ \to K^+K^-\pi^+$ decay mode in the exclusive analysis, efficiency of $D_s^+ \to K_S^0 K^+$ decay mode in the exclusive analysis, number of events observed in the exclusive analysis, product of vacuum polarization factor and ISR correction factor, inclusive cross section, and exclusive cross section, respectively. The uncertainties are statistical only.

$\sqrt{s}$ (GeV)	$\epsilon_{\rm inc}$ (%)	$N_{\rm inc}$	$\epsilon_{\rm exc}(D_s^+ \to K^+K^-\pi^+)$ (%)	$\epsilon_{\rm exc}(D_s^+ \to K_S^0 K^+)$ (%)	$N_{\rm exc}^{\rm obs}$	$\frac{1}{\lvert 1-\Pi\rvert^2}(1+\delta)$	$\sigma^{\rm inc}$(pb)	$\sigma^{\rm exc}$(pb)
4.600	30.2	159.5±25.2	9.3	13.6	28.9±5.7	0.79	21.1±3.3	9.7 ±1.9
4.620	29.1	113.1±26.0	7.9	11.1	16.2±4.6	0.95	14.5±3.3	6.1 ±1.7
4.640	29.3	139.6±27.0	8.1	11.3	17.3±4.4	0.88	18.3±3.5	6.5 ±1.6
4.660	29.2	111.4±27.7	7.6	10.4	11.6±4.0	1.02	13.1±3.3	4.2 ±1.4
4.680	29.3	289.5±50.0	7.4	10.2	30.4±6.1	1.02	10.7±1.9	3.5 ±0.7
4.700	29.3	126.3±28.6	7.8	10.6	10.4±3.7	1.0	15.0±3.4	3.7 ±1.3

TABLE III. The measured cross sections for $e^+e^- \to D_s^+ D_{s2}^*(2573)^-$. Definitions of each symbol are the same as those in Table II.

$\sqrt{s}$ (GeV)	$\epsilon_{\rm inc}$ (%)	$N_{\rm inc}$	$\epsilon_{\rm exc}(D_s^+ \to K^+K^-\pi^+)$ (%)	$\epsilon_{\rm exc}(D_s^+ \to K_S^0 K^+)$ (%)	$N_{\rm exc}^{\rm obs}$	$\frac{1}{\lvert 1-\Pi\rvert^2}(1+\delta)$	$\sigma^{\rm inc}$(pb)	$\sigma^{\rm exc}$(pb)
4.600	30.2	341.8±43.7	15.6	13.6	94.8±11.0	0.76	47.0±6.0	19.7±2.3
4.620	29.2	381.8±44.3	14.3	11.1	96.1±11.1	0.77	60.5±7.0	24.5±2.8
4.640	29.4	356.7±46.7	13.1	11.3	71.5±10.1	0.95	42.9±5.6	15.1±2.1
4.660	29.2	266.5±44.6	12.6	10.4	59.3±10.5	0.88	36.2±6.1	14.6±2.6
4.680	29.4	721.0±86.7	11.1	10.2	109.6±14.6	1.06	25.7±3.1	8.1 ±1.1
4.700	29.3	158.8±53.4	9.3	10.6	19.1±7.0	1.32	14.2±4.8	4.2 ±1.5

$$L_{i,j}^{\rm exc}(\sigma_{i,j}^{\rm exc}, \delta_{i,j}^{\rm exc}, \sigma_{i,j}, \mathcal{B}_i) = \frac{1}{\sqrt{2\pi}\delta_{i,j}^{\rm exc}} e^{-\frac{(\sigma_{i,j}^{\rm exc} - \sigma_{i,j}\mathcal{B}_i)^2}{2(\delta_{i,j}^{\rm exc})^2}}. \tag{3}$$

IV. FIT TO MEASURED CROSS SECTION

To study the resonance structures in the $e^+e^- \to D_s^+ D_{s1}(2536)^-$ and $e^+e^- \to D_s^+ D_{s2}^*(2573)^-$ processes, least-χ^2 fits to the measured cross sections are performed. The cross sections are described with the coherent sum of two constant width Breit-Wigner (BW) functions,

$$\sigma(\sqrt{s}) = |BW_0(\sqrt{s}) + BW_1(\sqrt{s})e^{i\phi_1}|^2. \tag{4}$$

$$BW_k(\sqrt{s}) = \frac{\sqrt{12\pi\Gamma_k^{\rm tot}\Gamma_k^{e^+e^-}\mathcal{B}_k}}{s - M_k^2 + iM_k\Gamma_k^{\rm tot}} \frac{\sqrt{\Phi(\sqrt{s})}}{\sqrt{\Phi(M_k)}}, \tag{5}$$

$$\Phi(\sqrt{s}) = \frac{q(\sqrt{s})^{2l+1}}{s}, \tag{6}$$

where M_k, $\Gamma_k^{\rm tot}$, and $\Gamma_k^{e^+e^-}$ are the mass, width, and electronic partial width of the $k^{\rm th}$ structure (R_k), respectively; $\mathcal{B}_k$ is the branching fraction of the decay $R_k \to D_s^+ D_{s1}(2536)^-/D_s^+ D_{s2}^*(2573)^-$, ϕ is the relative phase between R_1 and R_0, $q(\sqrt{s})$ is the momentum of D_s^+ in the rest frame of R_k, $\Phi(\sqrt{s})$ is the phase space factor of the two-body decay, and l is the angular momentum of $R_k \to D_s^+ D_{s1}(2536)^-/D_s^+ D_{s2}^*(2573)^-$.

The angular distribution of the $e^+e^- \to D_s^+ D_{s1}(2536)^-$ process is described by $1 + \alpha\cos^2\theta$, where $\alpha = -0.65 \pm 0.22$ is measured with our data. This indicates both S-wave and D-wave contributions exist, however, their fractions cannot be determined precisely due to the low statistics. We assume a pure D-wave process in the nominal fit and take a pure S-wave alternatively to estimate the systematic uncertainty. The $e^+e^- \to D_s^+ D_{s2}^*(2573)^-$ is pure D-wave.

In the analysis of $e^+e^- \to D_s^+ D_{s1}(2536)^-$, the mass and width of BW_0 are determined to be $M_0 = (4584 \pm 14 \pm 68)$ MeV/c^2 and $\Gamma_0^{\rm tot} = (57 \pm 12 \pm 211)$ MeV and those of BW_1 are $M_1 = (4749.9 \pm 8.2 \pm 6.7)$ MeV/c^2 and $\Gamma_1^{\rm tot} = (24.9 \pm 8.0 \pm 7.8)$ MeV, where the first uncertainties are statistical and the second systematic. In the analysis of $e^+e^- \to D_s^+ D_{s2}^*(2573)^-$, the mass and width of BW_0 are determined to be $M_0 = (4603.1 \pm 3.9 \pm 0.8)$ MeV/c^2 and $\Gamma_0^{\rm tot} = (45.2 \pm 5.7 \pm 0.7)$ MeV and those of BW_1 are $M_1 = (4720 \pm 13 \pm 2)$ MeV/c^2 and $\Gamma_1^{\rm tot} = (50 \pm 12 \pm 1)$ MeV.

V. SYSTEMATIC UNCERTAINTY

A. Absolute branching fraction measurement

The systematic uncertainties from $B_{\rm Other\ B.K.G.}$ in the 2D fit are estimated as 2.1% and 3.0% for $D_{s1}(2536)^- \to \bar{D}^{*0}K^-$ and $D_{s2}^*(2573)^- \to \bar{D}^0 K^-$, respectively, by sampling the cross sections of the process in $B_{\rm Other\ B.K.G.}$ 500 times according to their uncertainties.

The systematic uncertainties from fit range of $RM(D_s^+)$ in inclusive (exclusive) analyses are estimated by the "Barlow-test" [8, 9] as 0.1% and 0.7% (1.1% and 0.8%) for $D_{s1}(2536)^- \to \bar{D}^{*0}K^-$ and $D_{s2}^*(2573)^- \to \bar{D}^0 K^-$, respectively.

The parameters of the convolved Gaussian function in the 2D fit are changed by one standard deviation, and the largest changes are taken as the systematic uncertainty as 2.5% and 3.6% for $D_{s1}(2536)^- \to \bar{D}^{*0}K^-$ and $D_{s2}^*(2573)^- \to \bar{D}^0 K^-$, respectively.

The background shape of $M(K^-K^+\pi^+)$ in the 2D fit is changed from the first order Chebychev polynomial function to a second order one, and the systematic uncertainties are estimated as 5.0% and 7.4% for $D_{s1}(2536)^- \to \bar{D}^{*0}K^-$ and $D_{s2}^*(2573)^- \to \bar{D}^0 K^-$, respectively.

The background shape of $RM(D_s^+)$ in the 2D fit is changed from an ARGUS function to $f(M) = (M - M_a)^c (M_b - M)^d$, where c and d are floating parameters, and M_a (M_b) is the lower (upper) limit of mass distribution, which is fixed as $M_a = 0$ ($M_b = \sqrt{s} - m_{D_s^+}$) [5]. The systematic uncertainties are estimated as 1.0% and 1.6% for $D_{s1}(2536)^- \to \bar{D}^{*0}K^-$ and $D_{s2}^*(2573)^- \to \bar{D}^0 K^-$, respectively.

B. Exclusive cross section measurement

The systematic uncertainties of the $RM(D_s^+)$ fit range are estimated the same way as in the estimation of the absolute branching fraction measurements as 1.7% and 0.3% for $e^+e^- \to D_s^+ D_{s1}(2536)^-$ and $e^+e^- \to D_s^+ D_{s2}^*(2573)^-$, respectively.

The background shape of $RM(D_s^+)$ is changed from the first order Chebychev polynomial function to a second order one.

All the systematic uncertainties are shown in Tables IV and V.

C. Fit to measured cross section

The systematic uncertainties in the resonance parameters of R_0 and R_1 mainly stem from the center-of-mass energy measurement, center-of-mass energy spread, and systematic uncertainty of the cross sections.

The center-of-mass energies of data samples with $\sqrt{s} < 4.61$ GeV are measured with dimuon events with an uncertainty of ± 0.8 MeV [1], while those with $\sqrt{s} > 4.6$ GeV are measured with $\Lambda_c^+ \bar{\Lambda}_c^-$ events with an uncertainty of ± 0.6 MeV [2]. Thus 0.8 MeV is taken as the systematic uncertainty, and propagates to the masses of BW_0 and BW_1 by the same amount.

The systematic uncertainty from the center-of-mass energy spread is estimated by convolving the fit formula with a Gaussian function with a width of 1.6 MeV, which is the energy spread determined from the measurement results of the Beam Energy Measurement System [7].

The systematic uncertainties from the cross section measurement uncommon among data samples will influence the masses and widths of R_0 and R_1, which include ISR correction, background shape of $RM(D_s^+)$, and tracking and PID efficiencies of K^- not from D_s^+. The corresponding systematic uncertainty is estimated by including the uncertainty in the fit to the cross section, and taking the differences on the parameters as the systematic uncertainties.

The fraction of the S-wave and D-wave in the $e^+e^- \to D_s^+ D_{s1}(2536)^-$ decay also has influence on the results; conservatively, we assume S-wave is dominant, and the difference from the nominal fit is taken as the systematic uncertainty.

TABLE IV. Relative systematic uncertainty (%) in the exclusive cross section measurement for $e^+e^- \to D_s^+ D_{s1}(2536)^-$.

$\sqrt{s}$ (GeV)	4.600	4.610	4.620	4.640	4.660	4.680	4.700	4.740	4.750	4.780	4.840	4.914	4.946
Fit range (exc)	1.7	1.7	1.7	1.7	1.7	1.7	1.7	1.7	1.7	1.7	1.7	1.7	1.7
Mass window ($M(D_s^+)$)	3.4	3.4	3.4	3.4	3.4	3.4	3.4	3.4	3.4	3.4	3.4	3.4	3.4
Mass window ($RM(D_s^+K^-)$)	4.3	4.3	4.3	4.3	4.3	4.3	4.3	4.3	4.3	4.3	4.3	4.3	4.3
Tracking & PID ((tracks from D_s^+))	1.9	1.9	1.9	1.9	1.9	1.9	1.9	1.9	1.9	1.9	1.9	1.9	1.9
Tracking & PID ($K^\pm$ not from D_s^+)	1.7	1.5	1.4	1.6	1.3	1.2	1.1	0.9	0.9	0.8	0.8	0.8	0.8
$\mathcal{B}(D_s^+ \to K^+K^-\pi^+)$	1.9	1.9	1.9	1.9	1.9	1.9	1.9	1.9	1.9	1.9	1.9	1.9	1.9
$\mathcal{B}(D_s^+ \to K_S^0 K^+)$	2.4	2.4	2.4	2.4	2.4	2.4	2.4	2.4	2.4	2.4	2.4	2.4	2.4
B.K.G. shape (exc: $RM(D_s^+)$)	4.7	3.6	9.2	6.1	5.9	0.4	0.6	0.4	8.1	6.0	6.8	8.2	13.4
VVS_PWave	0.2	0.2	0.2	0.2	0.2	0.2	0.2	0.2	0.2	0.2	0.2	0.2	0.2
AngSam	3.3	3.3	3.3	3.3	3.3	3.3	3.3	3.3	3.3	3.3	3.3	3.3	3.3
ISR	1.4	3.5	3.6	1.9	2.2	1.7	2.0	3.2	1.1	1.0	0.9	0.4	2.3
Luminosity	1.0	1.0	1.0	1.0	1.0	1.0	1.0	1.0	1.0	1.0	1.0	1.0	1.0
Total	9.2	9.2	12.5	10.1	10.0	7.9	8.0	8.3	11.2	9.8	10.3	11.2	15.6

TABLE V. Relative systematic uncertainty (%) in the exclusive cross section measurement for $e^+e^- \to D_s^+ D_{s2}^*(2573)^-$.

$\sqrt{s}$ (GeV)	4.600	4.610	4.620	4.640	4.660	4.680	4.700	4.740	4.750	4.780	4.840	4.914	4.946
Fit range (exc)	0.3	0.3	0.3	0.3	0.3	0.3	0.3	0.3	0.3	0.3	0.3	0.3	0.3
Mass window ($M(D_s^+)$)	5.5	5.5	5.5	5.5	5.5	5.5	5.5	5.5	5.5	5.5	5.5	5.5	5.5
Mass window ($RM(D_s^+K^-)$)	4.3	4.3	4.3	4.3	4.3	4.3	4.3	4.3	4.3	4.3	4.3	4.3	4.3
Tracking & PID ((tracks from D_s^+))	1.9	1.9	1.9	1.9	1.9	1.9	1.9	1.9	1.9	1.9	1.9	1.9	1.9
Tracking & PID ($K^\pm$ not from D_s^+)	0.1	0.1	0.0	0.0	0.0	0.1	0.1	0.1	0.0	0.1	0.0	0.1	0.1
$\mathcal{B}(D_s^+ \to K^+K^-\pi^+)$	1.9	1.9	1.9	1.9	1.9	1.9	1.9	1.9	1.9	1.9	1.9	1.9	1.9
$\mathcal{B}(D_s^+ \to K_S^0 K^+)$	2.4	2.4	2.4	2.4	2.4	2.4	2.4	2.4	2.4	2.4	2.4	2.4	2.4
B.K.G. shape (exc: $RM(D_s^+)$)	3.0	6.5	5.4	13.4	5.5	8.8	7.0	2.5	4.1	7.2	13.0	46.3	25.8
ISR	1.0	2.7	1.1	1.3	0.8	1.2	2.9	5.3	2.5	0.7	0.6	0.6	1.6
Luminosity	1.0	1.0	1.0	1.0	1.0	1.0	1.0	1.0	1.0	1.0	1.0	1.0	1.0
Total	8.5	10.6	9.7	15.6	9.7	11.9	11.0	9.9	9.3	10.7	15.2	47.0	27.0

TABLE VI. The measured cross sections for $e^+e^- \to D_s^+ D_{s1}(2536)^-$ in the exclusive analysis by the counting method. $N_{\rm exc}^{\rm count}$ is the number of events obtained by the counting method. The uncertainties for $N_{\rm exc}^{\rm count}$ and $\sigma^{\rm exc}$ are statistical only.

$\sqrt{s}$ (GeV)	$\epsilon_{\rm exc}(D_s^+ \to K^+K^-\pi^+)$ (%)	$\epsilon_{\rm exc}(D_s^+ \to K_S^0 K^+)$ (%)	$N_{\rm exc}^{\rm count}$	$\frac{1}{\lvert 1-\Pi \rvert^2}(1+\delta)$	$\sigma^{\rm exc}$(pb)
4.530	10.2	15.1	$3.0^{+46.5}_{-14.5}$	0.7	$0.6^{+9.0}_{-2.8}$
4.575	9.4	13.8	$0.3^{+27.5}_{-0.0}$	0.8	$0.1^{+11.2}_{-0.0}$

The systematic uncertainties in the measured resonance parameters are shown in Tables X $\sim$ XI.

[1] M. Ablikim *et al.* (BESIII Collaboration), Chin. Phys. C **40**, 063001 (2016).
[2] M. Ablikim *et al.* (BESIII Collaboration), Chin. Phys. C **46**, 113003 (2022).
[3] M. Ablikim *et al.* (BESIII Collaboration), Chin. Phys. C **46**, 113002 (2022).
[4] M. Ablikim *et al.* (BESIII Collaboration), Phys. Rev. Lett. **131**, 151903 (2023).
[5] M. Ablikim *et al.* (BESIII Collaboration), Phys. Rev. D **101**, 112008 (2020).

TABLE VII. The measured cross sections for $e^+e^- \to D_s^+ D_{s1}(2536)^-$ in the exclusive analysis. The first uncertainties for $N_{\rm exc}^{\rm obs}$ and $\sigma^{\rm exc}$ are statistical and the second ones for $\sigma^{\rm exc}$ are systematic.

$\sqrt{s}$ (GeV)	$\epsilon_{\rm exc}(D_s^+ \to K^+K^-\pi^+)$ (%)	$\epsilon_{\rm exc}(D_s^+ \to K_S^0 K^+)$ (%)	$N_{\rm exc}^{\rm obs}$	$\frac{1}{\lvert 1-\Pi\rvert^2}(1+\delta)$	$\sigma^{\rm exc}$(pb)
4.600	9.4	13.6	28.9±5.7	0.79	9.7 ±1.9 ±0.9
4.610	9.3	12.2	4.6 ±2.3	0.83	9.1 ±4.4 ±0.8
4.620	8.7	11.1	16.2±4.6	0.95	6.1 ±1.7 ±0.8
4.640	7.9	11.3	17.3±4.4	0.88	6.5 ±1.6 ±0.7
4.660	8.1	10.4	11.6±4.0	1.02	4.2 ±1.4 ±0.4
4.680	7.6	10.2	30.4±6.1	1.02	3.5 ±0.7 ±0.3
4.700	7.4	10.6	10.4±3.7	1.0	3.7 ±1.3 ±0.3
4.740	7.8	12.8	7.5 ±3.0	0.95	7.5 ±3.0 ±0.6
4.750	9.5	14.0	31.6±5.9	0.71	17.6±3.3 ±2.0
4.780	10.2	12.0	26.7±5.5	0.96	9.2 ±1.9 ±0.9
4.840	8.8	10.3	13.9±4.0	1.12	4.5 ±1.3 ±0.5
4.914	7.9	12.2	11.1±3.6	0.88	9.5 ±3.1 ±1.1
4.946	9.6	9.8	4.4 ±2.4	1.15	4.6 ±2.5 ±0.7

TABLE VIII. The measured cross sections for $e^+e^- \to D_s^+ D_{s2}^*(2573)^-$ in the exclusive analysis by the counting method. $N_{\rm exc}^{\rm count}$ is the number of events obtained by the counting method. The uncertainties for $N_{\rm exc}^{\rm count}$ and $\sigma^{\rm exc}$ are statistical only.

$\sqrt{s}$ (GeV)	$\epsilon_{\rm exc}(D_s^+ \to K^+K^-\pi^+)$ (%)	$\epsilon_{\rm exc}(D_s^+ \to K_S^0 K^+)$ (%)	$N_{\rm exc}^{\rm count}$	$\frac{1}{\lvert 1-\Pi\rvert^2}(1+\delta)$	$\sigma^{\rm exc}$(pb)
4.575	16.2	24.5	$-0.5^{+10.1}_{-0.0}$	0.7	$-0.2^{+4.3}_{-0.0}$

[6] M. Ablikim *et al.* (BESIII Collaboration), Phys. Rev. D **104**, 032012 (2021).
[7] E.V. Abakumova *et al.*, Nucl. Instrum. Meth. A **659**, 21 (2011).
[8] R. Barlow, in *Conference on Advanced Statistical Techniques in Particle Physics* (2002) pp.134–144.
[9] M. Ablikim *et al.* (BESIII Collaboration), Nature **606**, 64 (2022).

TABLE IX. The measured cross sections for $e^+e^- \to D_s^+ D_{s2}^*(2573)^-$ process in the exclusive analysis. The first uncertainties for $N_{\rm exc}^{\rm obs}$ and $\sigma^{\rm exc}$ are statistical and the second ones for $\sigma^{\rm exc}$ are systematic.

$\sqrt{s}$ (GeV)	$\epsilon_{\rm exc}(D_s^+ \to K^+K^-\pi^+)$ (%)	$\epsilon_{\rm exc}(D_s^+ \to K_S^0 K^+)$ (%)	$N_{\rm exc}^{\rm obs}$	$\frac{1}{\lvert 1-\Pi\rvert^2}(1+\delta)$	$\sigma^{\rm exc}$(pb)
4.600	15.6	13.6	94.8±11.0	0.79	19.7±2.3 ±1.7
4.610	14.4	12.2	15.9±5.4	0.83	18.5±6.3 ±2.0
4.620	14.3	11.1	96.1±11.1	0.95	24.5±2.8 ±2.4
4.640	13.1	11.3	71.5±10.1	0.88	15.1±2.1 ±2.4
4.660	12.6	10.4	59.3±10.5	1.02	14.6±2.6 ±1.4
4.680	11.1	10.2	109.6±14.6	1.02	8.1 ±1.1 ±1.0
4.700	9.3	10.6	19.1±7.0	1.0	4.2 ±1.5 ±0.5
4.740	9.7	12.8	4.7 ±3.1	0.95	3.3 ±2.1 ±0.3
4.750	11.8	14.0	18.5±6.0	0.71	7.1 ±2.3 ±0.7
4.780	12.3	12.0	36.4±8.0	0.96	9.5 ±2.1 ±1.0
4.840	11.1	10.3	29.3±6.9	1.12	7.4 ±1.7 ±1.1
4.914	11.6	12.2	15.9±5.5	0.88	10.7±3.7 ±5.0
4.946	10.4	9.8	9.0 ±4.5	1.15	7.7 ±3.9 ±2.1

TABLE X. The systematic uncertainties in the measurement of the resonance parameters in the $e^+e^- \to D_s^+ D_{s1}(2536)^-$ process. $\sqrt{s}$ represents the systematic uncertainty from the center-of-mass energy measurement. Cross Section represents the systematic uncertainty from the cross section measurements which are uncommon among data samples. S-wave represents the systematic uncertainty from the S-wave decay of $D_s^+ D_{s1}(2536)^-$. The units of M_0 and $\Gamma_0^{\rm tot}$ are MeV/c^2 and MeV, respectively.

	$\sqrt{s}$	Center-of-mass Energy Spread	Cross Section	S-wave	Overall
M_0	0.8	7.3	7.8	67.1	67.9
$\Gamma_0^{\rm tot}$	-	3.9	3.7	211.3	211.4
M_1	0.8	4.7	4.7	0.5	6.7
$\Gamma_1^{\rm tot}$	-	3.5	4.1	5.7	7.8

TABLE XI. The systematic uncertainties in the measurement of the resonance parameters in the $e^+e^- \to D_s^+ D_{s2}^*(2573)^-$ process. $\sqrt{s}$ represents the systematic uncertainty from the center-of-mass energy measurement. Cross Section represents the systematic uncertainty from the cross section measurements which are uncommon among data samples. The units of M_1 and $\Gamma_1^{\rm tot}$ are MeV/c^2 and MeV, respectively.

	$\sqrt{s}$	Center-of-mass Energy Spread	Cross Section	Overall
M_0	0.8	0.0	0.1	0.8
$\Gamma_0^{\rm tot}$	-	0.2	0.7	0.7
M_1	0.8	0.2	1.3	1.5
$\Gamma_1^{\rm tot}$	-	0.2	0.9	0.9